On the Adequacy of Adams-Bashforth Sampled-Data Models for Characterizing Complex Underwater-Vehicle Dynamics with Noisy Measurements

Mario A. Jordán [1,2], Jorge L. Bustamante[1,2] and Carlos Berger[1,2]

[1] Argentinean Institute of Oceanography (IADO-CONICET).
Florida 8000, Complejo CCT, Edificio E1, B8000FWB,
Bahía Blanca, ARGENTINA.

[2] Dto. Ingeniería Eléctrica y de Computadoras- Univ. Nac. del Sur
(DIEC-UNS).
No Institute Given

Abstract. In this paper the adequacy of high order interpolation-based approaches to describe highly perturbed complex dynamics in discrete time was analyzed. The analysis establishes features of the approaches related to modularity, consistency with the model order and the sampling times, and accuracy in disturbed contexts with noisy measurements.
A detailed study of the sensitivity of local prediction errors under a high signal-to-noise ratio is carried out with analytical expressions in dependence of physical coefficients of the vehicle.
The different interpolation-based approaches were illustrated with simulations using from an AUV-like (Autonomous Underwater Vehicle) system with a few degrees of freedom (DoF), to a ROV (Remotely Operated Vehicle) model of 6 DoF with complex navigation paths.
Key words: Sampled-data models, Adams-Bashforth approximations, underwater vehicles, nonlinear dynamics, local errors, disturbances.

1 Introduction

Physical models for characterizing system dynamics in continuous time are typically available in the form of ordinary differential equations (ODEs) with eventually time-varying parameters. Translation of ODE-based descriptions to time-discrete models is an ineludible problem when applying digital technology to achieve designs of control system, parameter estimators and signal filters.

Generally, more and more ambitious requirements on accuracy in the operation of complex dynamic systems, give impetus to employ preferably such accurate models that can preserve the scope of the design goal across the steps in the synthesis. These, for instance, are the requirements pointed up in the design of guidance-navigation-control systems for a particular underwater vehicle dynamics, which must deal with actuating perturbations and strong nonlinearities due to inherent hydrodynamics and thruster characteristics [1]-[2].

Because it is not possible to analytically describe the exact discrete-time model of a nonlinear system, approximated digital models are a reasonable way to support the design of a digital control system.

The start point in this paper is the availability of the physical ODEs for the characterization of a vehicle dynamics. Our objective is to explore the adequacy for digital controller of certain ODE-related interpolation-based approximations, in contrast with the Euler Method that seemed as the most widespread in most applications in the research area [3]-[4]. The criterions of the analysis between the different methods are their features of modularity, consistency with the model order, accuracy in disturbed contexts and noisy measurements among others. We will pay attention to the model-performance dependence with respect to sensitivity functions that are in correspondence to certain physical coefficients.

Without entering the phase of any particular controller design, many suggestions could be given beforehand for the application of prediction-based models in a control context for vehicles and perturbations that occurs basically from sensors. Finally, a case study for a complex system dynamics in six degrees of freedom (DoF) will illustrate the features of some of presented High-order approximations in comparison to the Euler's Method for potential control applications.

2 Preliminaries

2.1 Continuous-time nonlinear dynamics

Many mechanical system dynamics are mathematically described by the interconnection of an ODE for the inertial part of the system together with an ODE for the kinematic part. Additionally, a nonlinear actuator characteristic is included and all parts connected blockwise as illustrated in Fig. 1.

The broad class we are referring to embraces mobile robots, unmanned aerial vehicles, spacecraft and satellite systems, autonomous underwater vehicles (AUV), and remotely operated vehicles (ROV) among others. Usually, the dynamics of a ROV may be the most complex one due to its non-linear hydrodynamics, high DoF, significant perturbations and measurement errors actuating on it. So the analysis here will be focused mainly to this complexity level.

In a general form, a vehicle dynamics can be described by

$$\dot{\mathbf{v}}=\mathbf{f}_v(\boldsymbol{\eta},\mathbf{v},\boldsymbol{\tau},\boldsymbol{\tau}_c) \tag{1}$$

$$\dot{\boldsymbol{\eta}}=\mathbf{f}_\eta(\boldsymbol{\eta},\mathbf{v},\mathbf{v}_c) \tag{2}$$

$$\mathbf{n}=\mathbf{f}_n(\mathbf{v},\mathbf{n}_r) \tag{3}$$

$$\boldsymbol{\tau}=\mathbf{f}_\tau(\mathbf{n},\mathbf{v}), \tag{4}$$

where $\boldsymbol{\eta}$ is the generalized position vector and $\mathbf{v}$ is the generalized rate vector. The vector $\boldsymbol{\tau}$ is the generalized propulsion vector applied on the vehicle. The vector $\mathbf{n}$ describes the angular velocities of the motors (particularly thrusters in ROVs) and $\mathbf{n}_r$ is the system input vector defining references for $\mathbf{n}$.

Usually, there exist perturbations acting on the dynamics such as a force perturbation $\boldsymbol{\tau}_c$ (for instance, the cable tug in ROVs) and a velocity perturbation $\mathbf{v}_c$ (for instance, the one due to fluid current or wind rates). Additionally, for design and stability analysis in control systems one has to consider disturbances $\delta\mathbf{v}$ and $\delta\boldsymbol{\eta}$ for the measured kinematic and spatial states, respectively.

The right members $\mathbf{f}_v$, $\mathbf{f}_\eta$, $\mathbf{f}_n$ and $\mathbf{f}_\tau$ in (1)-(4) are non-linear vector functions describing the inertia, kinematics, actuator dynamics and actuator statics in

this order. A scope of available model structures and details of marine systems is given in [1]. For further analysis we will generally specify

$$\mathbf{f}_v = M^{-1}\left(-C(\mathbf{v})\mathbf{v} - D(|\mathbf{v}|)\mathbf{v} + \mathbf{g}(\boldsymbol{\eta}) + \boldsymbol{\tau} + \boldsymbol{\tau}_c\right) \tag{5}$$

$$\mathbf{f}_\eta = J(\boldsymbol{\eta})\left(\mathbf{v} + \mathbf{v}_c\right) \tag{6}$$

$$\mathbf{f}_\tau = K_1 \mathbf{n}^T \mathbf{n} - K_2 \mathbf{v}^T \mathbf{n}, \tag{7}$$

where matrices M, C, and D represent the inertia, the Coriolis and centripetal forces, and the damping, respectively, $\mathbf{g}$ the buoyancy vector and $J(\boldsymbol{\eta})$ the rotation matrix. All the arrays C, D, J and $\mathbf{g}$ are nonlinearly state-dependent on $\mathbf{v}$ and $\boldsymbol{\eta}$, while K_1 and K_2 are constant matrices that depend on thrust system. The vector function $\mathbf{f}_n$ in (3) is generally characterized with transfer-functions corresponding to a set of tachometric control loops.

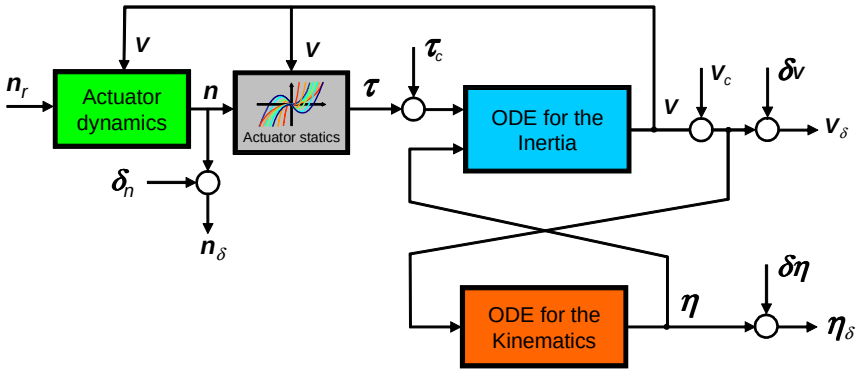

Fig. 1 - Physical model structure for a vehicle dynamics with perturbations and noisy measurements of the states

2.2 Sampled-data dynamics

For the continuous-time dynamics there exists an exact sampled-data dynamics described by the set of sequences $\{\boldsymbol{\eta}(t_i), \mathbf{v}(t_i), \mathbf{n}(t_i), \mathbf{n}_r(t_i)\}$ for the states $\boldsymbol{\eta}$, $\mathbf{v}$, $\mathbf{n}$ and the input $\mathbf{n}_r$ at times t_i with a sampling rate h. Complementary the vehicle behavior is characterized in discrete time through the noisy measurements in the sequence set $\{\boldsymbol{\eta}_\delta(t_i), \mathbf{v}_\delta(t_i), \mathbf{n}_\delta(t_i), \mathbf{n}_r(t_i)\}$ as illustrated in Fig. 1.

3 Discretization methods

In this paper, considering the well-known vehicles dynamics, we are going into details in interpolation-based methods that take full advantage of the phenomenological structure of the ODE system. We now summarize some known results from the area of Numerical Simulation taking the most extended algorithms and the generic ODE $\dot{\mathbf{x}}$=$\mathbf{f}$($\mathbf{x}$,$\mathbf{u}$) as support [5].

Euler and Tustin approximations The Euler transformation implements a forward difference of the first time derivative $\mathbf{x}_{n+1} = \mathbf{x}_n + h\ \mathbf{f}(\mathbf{x}_n, \mathbf{u}_n)$.

Another transformation, which corresponds to the trapezoidal method for numerical integration, is the Tustin or bilinear approximation. The difference with the Euler method is that this is an implicit method while the Euler is not.

Runge-Kutta approximations This methods perform multiple evaluations of $\mathbf{f}$ in each integration subinterval as required for a given accuracy. There exists

a family of explicit and implicit Runge-Kutta methods that compute approximations to $\mathbf{x}(t)$ with initial value $\mathbf{x}(t_0)$ using the Taylor series expansion about t_n. Such an explicit approximation of order s is a weighted average defined as

$$\mathbf{x}_{n+1} = \mathbf{x}_n + h\left(b_1\mathbf{k}_1 + \cdots + b_s\mathbf{k}_s\right), \tag{8}$$

with $\mathbf{k}_i$ being slopes of the path $\mathbf{x}(t)$.

Adams-Bashforth approximations This method is an explicit multistep linear method that performs an approximation of $\mathbf{x}(t)$ with initial value $\mathbf{x}(t_0)$ at $t = t_{n+1} = t_0 + (n+1)h$ with $n = 0, 1, 2, ...$ based on a linear combination of samples $\mathbf{f}(\mathbf{x}_i, \mathbf{u}(t_i))$ from $i = n$ up to $i = n - s + 1$.

The coefficients of the linear combination are obtained by using the Lagrange formula for polynomial interpolation. The order of accuracy per step is equal to s, *i.e.*, $\mathbf{x}(t_{n+1}) - \mathbf{x}_{n+1} \in \mathcal{O}(h^{s+1})$.

More details about the stability of Adam-Bashforth and other methods are given in many books oriented to Numerical Analysis, see for instance [6].

4 Approximation comparison

In this section we attempt to elucidate advantages and drawbacks of the different approximations described before employing a simple case study. This will enable us in a simple but categorical way to establish criteria to a suitably selection of sampled-data models for design purposes of digital controllers.

4.1 A simple case study

To this end, let us considered the following system accounting for a simple dynamics similar to an AUV ODE system restricted to a few DoF

$$\dot{y} = \alpha y^2 + \beta y + \gamma y\left|y\right| + \delta \sin^2(x) + u_1 \tag{9}$$

$$\dot{x} = -\sin^2(x)\, y, \tag{10}$$

with states x and y for position and velocity, respectively, the term βy^2s being in similitude with a Coriolis-centripetal acceleration, the terms βy and $\gamma y\left|y\right|$ playing the role of the linear and quadratic drag terms, and finally $\delta \sin^2(x)$ resembling the buoyancy in a combined pitch-roll motion. The term u_1 accounts for the excitation from thrusters. The term $\sin^2(x)\, y$ in (10) reflect the effect of the rotation matrix J for the combined pitch-roll motion.

For simulation purposes, the dynamics coefficients were set up $\alpha = -0.1$, $\beta = -0.05$, $\gamma = -0.2$ and $\delta = 0.5$. These values were selected in order to allow the nonlinear terms to have similar order of magnitudes. The input u_1 was suitably chosen in order to cause persistent excitation of the dynamics. For this goal, a random multilevel signal was proposed with a statistically uniform distribution of the amplitude levels. The sampling time was fixed sufficiently small according to the most rapid dynamics of the system (9)-(10).

4.2 Numerical simulation and estimation

Preliminaries The start point for an approximation comparison is the obtaining of an exact sampled-data model for the ODE system (9)-(10), which is numerically simulated and their states sampled at a rate h. Parallel, the one-step-ahead predictor of any presented approximation is run and fed with the sampled data.

To distinguish the methods the following notation is used, namely: Euler (E), estimated Euler (Ee), Tustin (T), Adams-Bashforth (AB), estimated Adams-Bashforth (ABe), Runge-Kutta (RK).

The set of parameters for the case study embraces those for the discrete-time model structure, excitation and estimation separately.

So, the structural model parameters are represented by the approximation order s. They are indicated by suffixes next to the approach label, *e.g.*, RK_s will mean the Runge-Kutta approximation of order s.

On the other hand, the set-up for the excitation u_1 is characterized by the choice of the h_u/h, with h_u is the step length at any signal level. For $h_u/h = 1$, u_1 will look like a white noise, and for increasing rate the signal becomes more predictable. The amplitude levels of u_1 are in the range of ± 10.

The parameter estimation (when applies) is defined by the identification in the stationary state, minimizing a Lebesgue series norm for the local error.

Results The main results of the study are summarized in Figs. 2 and 3 that illustrate the evolutions of the local errors in logarithmic scale.

As seen in Fig. 2 the AB approximation is consistent with the order s (it is, the larger the order the better the prediction quality in terms of the norm). For the ABe approximation there is no improvement with increasing orders.

Quite precise and consistent looked the RK methods, see Fig. 3. The difference in quality between them and the simple Euler approximation is significant in various order of magnitudes.

4.3 Feature comparison in view of controller designs

Often nonlinear systems require complex nonlinear controllers. So, in order to keep the scope of the controller design matching this complexity, some modularity of the model is quite important. Moreover, it is desirable for the sake of design simplicity that a discrete-time model has the associated prediction sampling period equal to the control sampling period. Additionally, even when some discrete-time models can manifest unstable global behavior, this property is not relevant in controller design because they usually involve a finite number of steps for an ahead prediction (usually one step) with bounded local errors. Quite important is that this prediction error is usually reflected in the appearance of compact residual sets in the tracking problem of vehicles (see [7]).

From the point of view of modularity, it seems that all approximations offer flexibility in the model structure. AB approximations do increase the complexity of modeling and parameter identification linearly with s, involving about s times more computations than the Euler method. On the other hand, for RK models the computational effort increases proportional to s^2 with a need of intersampling. It should be noticed that the Euler method is equivalent to the AB and the RK approximations with an order $s = 1$.

In summary, from model adequacy for control purposes, the explicit calculation of the one-step-ahead prediction on the basis of present and past control values shows again the Euler and AB methods as convenient approaches. Because of their superior adequacy for controller design, we will focus from now on the AB approximations for further analysis on more complex dynamics.

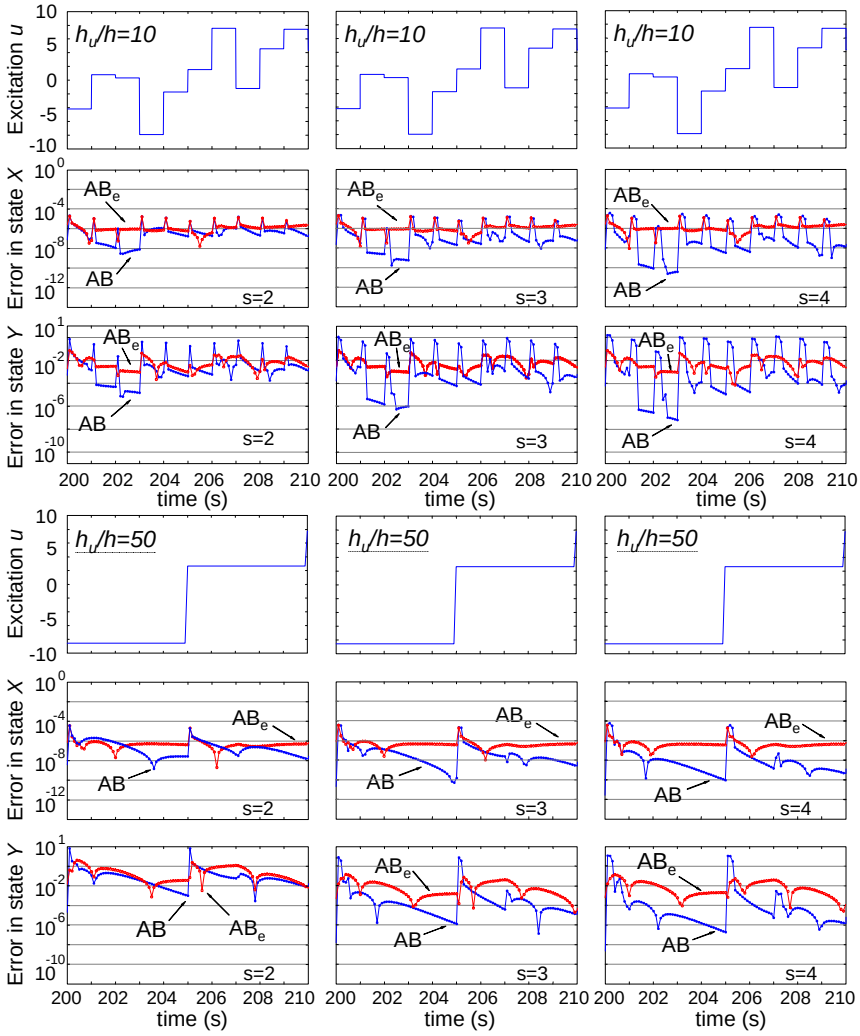

Fig. 2 - Local error evolution in Adams-Bashforth approximations for different s and h_u/h

5 Measurement Errors

Focusing on the previously selected AB approach, the goal in this section is to establish relations between local model with measurement errors and with physical parameters of the underwater vehicle. Afterwards, we will evaluate the sensitivity of spatial and kinematics model errors with respect to changes of these parameters and subject to operations which are typical of these systems.

In our analysis we will focus the most common case that appears when the non-autonomous dynamics (1)-(2) of an underwater vehicle is dominant in front of the actuator dynamics (3). Additionally, without loss of generality, we consider inertial and kinematic perturbations $\boldsymbol{\tau}_c$ and $\mathbf{v}_c$ null.

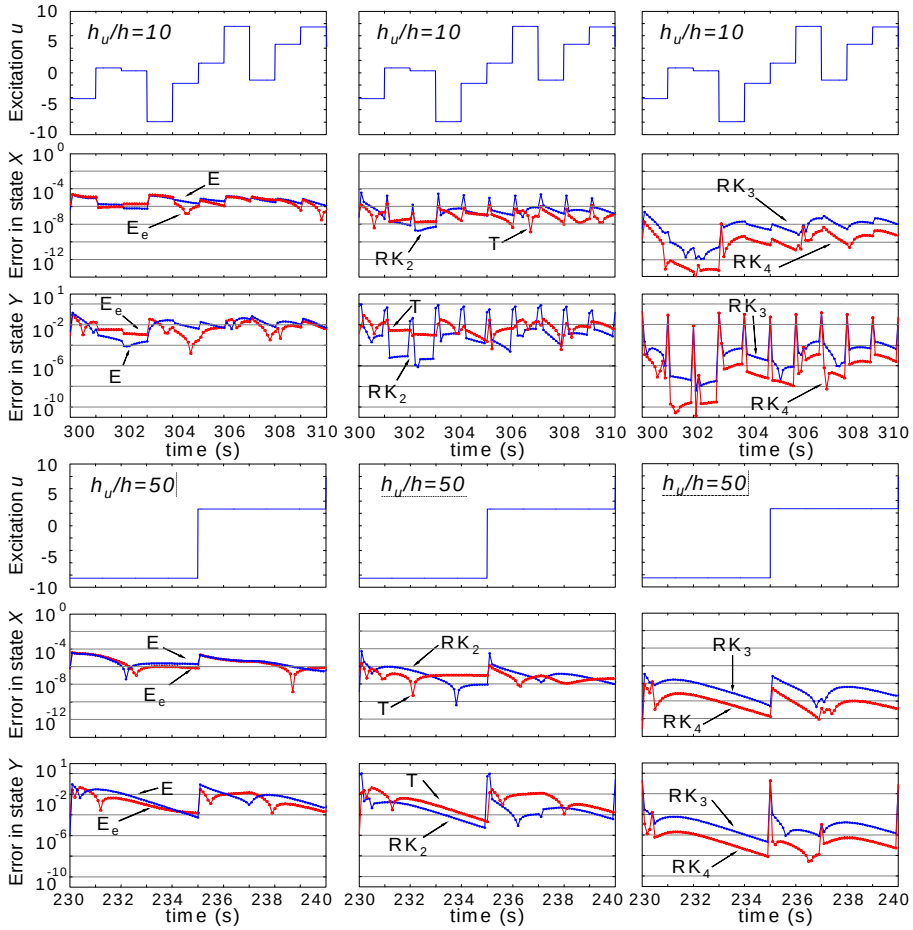

Fig. 3 - Local error evolution in Euler, Runge-Kutta and Tustin approximations for different s and h_u/h

5.1 Disturbed local error

We define now disturbed local errors as $\bar{\boldsymbol{\varepsilon}}_{v_{n+1}}=\mathbf{v}(t_{n+1}) + \delta\mathbf{v}_{n+1}-\mathbf{v}_{n+1}$ and $\bar{\boldsymbol{\varepsilon}}_{\eta_{n+1}}=\boldsymbol{\eta}(t_{n+1}) + \delta\boldsymbol{\eta}_{n+1}-\boldsymbol{\eta}_{n+1}$.

Assuming bounded noise vectors $\delta\mathbf{v}_i$ and $\delta\boldsymbol{\eta}_i$ we can expand $\mathbf{v}(t_{n-i+1})$ and $\boldsymbol{\eta}(t_{n-i+1})$ in series of Taylor about the values of undisturbed measures . So it is accomplished

$$\bar{\boldsymbol{\varepsilon}}_{v_{n+1}} = \boldsymbol{\varepsilon}_{v_{n+1}}+\Delta\delta\mathbf{v}_{n+1}-\sum_{i=1}^{s} a_i \left(\frac{\partial \mathbf{f}_v^T}{\partial \mathbf{v}}(t_{n-i+1})\delta\mathbf{v}_{n-i+1}+ \right. \tag{11}$$

$$\left. +\frac{\partial \mathbf{f}_v^T}{\partial \boldsymbol{\eta}}(t_{n-i+1})\delta\boldsymbol{\eta}_{n-i+1}+\frac{\partial \mathbf{f}_v^T}{\partial \mathbf{f}_\tau}\frac{\partial \mathbf{f}_\tau^T}{\partial \mathbf{v}}(t_{n-i+1})\delta\mathbf{v}_{n-i+1}+\mathbf{o}_i(\delta\mathbf{v}^2)+\mathbf{o}_i(\delta\boldsymbol{\eta}^2)\right)$$

$$\bar{\varepsilon}_{\eta_{n+1}} = \varepsilon_{\eta_{n+1}} + \Delta\delta\boldsymbol{\eta}_{n+1} - \sum_{i=1}^{s} a_i \left(\frac{\partial \mathbf{f}_\eta^T}{\partial \mathbf{v}}(t_{n-i+1})\delta\mathbf{v}_{n-i+1} + \right. \tag{12}$$
$$\left. + \frac{\partial \mathbf{f}_\eta^T}{\partial \boldsymbol{\eta}}(t_{n-i+1})\delta\boldsymbol{\eta}_{n-i+1} + \mathbf{o}_i(\delta\mathbf{v}^2) + \mathbf{o}_i(\delta\boldsymbol{\eta}^2) \right),$$

where $\varepsilon_{v_{n+1}}$ and $\varepsilon_{\eta_{n+1}}$ are the model local errors which are completely lacking in the influence of sampled-data disturbances, and one accomplishes $\Delta\delta\mathbf{v}_{n+1} = \delta\mathbf{v}_{n+1} - \delta\mathbf{v}_n$ and $\Delta\delta\boldsymbol{\eta}_{n+1} = \delta\boldsymbol{\eta}_{n+1} - \delta\boldsymbol{\eta}_n$. The functions $\mathbf{o}_i$ are truncating error vectors of the Taylor series expansions, all of them belonging to $\mathcal{O}(h^{s+1})$. Moreover, $\frac{\partial \mathbf{f}_v^T}{\partial \mathbf{v}}$ and $\frac{\partial \mathbf{f}_v^T}{\partial \boldsymbol{\eta}}$ are Jacobian matrices of the system which act as variable gains that propagate the sampled-data disturbances along the path.

5.2 Sensitivity

The Jacobians components are from (5)-(7)

$$\frac{\partial \mathbf{f}_v^T}{\partial \mathbf{v}} = -M^{-1}\left(\frac{\partial \mathbf{v}^T C^T(\mathbf{v})}{\partial \mathbf{v}} + \frac{\partial \mathbf{v}^T D^T(|\mathbf{v}|)}{\partial \mathbf{v}} \right) \tag{13}$$

$$\frac{\partial \mathbf{f}_v^T}{\partial \boldsymbol{\eta}} = M^{-1}\frac{\partial \mathbf{g}^T}{\partial \boldsymbol{\eta}} \tag{14}$$

$$\frac{\partial \mathbf{f}_v^T}{\partial \mathbf{f}_\tau} = M^{-1} \tag{15}$$

$$\frac{\partial \mathbf{f}_\tau^T}{\partial \mathbf{v}} = -\mathbf{n}^T K_2 \tag{16}$$

$$\frac{\partial \mathbf{f}_\eta^T}{\partial \mathbf{v}} = J(\boldsymbol{\eta}) \tag{17}$$

$$\frac{\partial \mathbf{f}_\eta^T}{\partial \boldsymbol{\eta}} = \frac{\partial \mathbf{v}^T J^T(\boldsymbol{\eta})}{\partial \boldsymbol{\eta}}, \tag{18}$$

If we closely analyze the bounds for the Jacobians in the state space of $\mathbf{v}$ and $\boldsymbol{\eta}$, we can conclude they are achieved at boundaries of the state domain. The following analytical expressions can be derived

$$\max_{\mathbf{v},\eta} \left\| \frac{\partial \mathbf{f}_v^T}{\partial \mathbf{v}} \right\| = \left\| \frac{\partial \mathbf{f}_v^T(\max\|\mathbf{v}\|)}{\partial \mathbf{v}} \right\| \tag{19}$$

$$\max_{\mathbf{v},\eta} \left\| \frac{\partial \mathbf{f}_v^T}{\partial \boldsymbol{\eta}} \right\| \leq \left\| M^{-1} \right\| \left\| \frac{\partial \mathbf{g}^T(\max|\varphi|, \max|\theta|)}{\partial \boldsymbol{\eta}} \right\| \tag{20}$$

$$\max_{\mathbf{v},\mathbf{n}} \left\| \frac{\partial \mathbf{f}_\tau^T}{\partial \mathbf{v}} \right\| \leq \|K_2\| \max\|\mathbf{n}\| \tag{21}$$

$$\max_{\mathbf{v},\eta} \left\| \frac{\partial \mathbf{f}_\eta^T}{\partial \mathbf{v}} \right\| = \|J(\max|\theta|)\| \tag{22}$$

$$\max_{\mathbf{v},\eta} \left\| \frac{\partial \mathbf{f}_\eta^T}{\partial \boldsymbol{\eta}} \right\| \leq \left\| \frac{\partial J^T(\max|\theta|)}{\partial \boldsymbol{\eta}} \right\| \max\|\mathbf{v}\|. \tag{23}$$

Clearly it is seen that noisy measures impact on the accuracy less in heavy vehicles than in light ones because of the inertia factor M^{-1} in (13)-(14). Moreover,

in vehicle maneuvers with broad changes of the pitch angle θ one may originate relatively large prediction errors even at slow motions, which would have to imply caution in the control actions of the guidance system designed upon this model. The reason for this effect is that the norms of J and $\frac{\partial J}{\partial \boldsymbol{\eta}}$ in (22)-(23) increase for large values of θ and particularly they are singular at $\theta = \pm\frac{\pi}{2}$. Finally one sees that the velocity affects the accuracy linearly as indicated in (18) and (23) but also nonlinearly (*cf.* (13) and (19)).

5.3 Model performance in the presence of noisy sampled data

Let us assume that there exist noisy measurements in velocity $\mathbf{v}$ and position $\boldsymbol{\eta}$. Let $\|\delta\mathbf{v}\|$ and $\|\delta\boldsymbol{\eta}\|$ be the bounds for the measurement errors. So with (11)-(22) it is valid

$$\left\|\bar{\boldsymbol{\varepsilon}}_{v_{n+1}}\right\| \leqslant \left\|\boldsymbol{\varepsilon}_{v_{n+1}}\right\| + 2\left\|\delta\mathbf{v}\right\| + \tag{24}$$
$$+a_s\left(\left(\left\|\frac{\partial \mathbf{f}_v^T(\max\|\mathbf{v}\|)}{\partial \mathbf{v}}\right\| + \left\|M^{-1}\right\|\left\|K_2\right\|\max\|\mathbf{n}\|\right)\|\delta\mathbf{v}\| + \right.$$
$$\left. + \left\|M^{-1}\right\|\left\|\frac{\partial \mathbf{g}^T(\max|\varphi|, \max|\theta|)}{\partial \boldsymbol{\eta}}\right\|\|\delta\boldsymbol{\eta}\|\right) + so_v + so_\eta$$

$$\left\|\bar{\boldsymbol{\varepsilon}}_{\eta_{n+1}}\right\| \leqslant \left\|\boldsymbol{\varepsilon}_{\eta_{n+1}}\right\| + 2\left\|\delta\boldsymbol{\eta}\right\| + a_s\left\|J(\max|\theta|)\right\|\left\|\delta\mathbf{v}\right\| + \tag{25}$$
$$+a_s\left\|\frac{\partial J_j^T(\max|\theta|)}{\partial \boldsymbol{\eta}}\right\|\left\|\mathbf{v}\right\|_n\left\|\delta\boldsymbol{\eta}\right\|_n + so_v + so_\eta$$

where o_v and o_η are the maximal norms of all the truncation error vectors $\mathbf{o}_i(\delta\mathbf{v}^2)$ and $\mathbf{o}_i(\delta\boldsymbol{\eta}^2)$, respectively, and the coefficient a_s is equal to $\sum_{i=1}^{s}|a_i|$.

Since $\boldsymbol{\varepsilon}_{v_{n+1}}$ and $\boldsymbol{\varepsilon}_{\eta_{n+1}}$ also belong to $\mathcal{O}(h^{s+1})$, they go to zero exponentially for increasing s. On the contrary, it is noticing from (24)-(25) that the contribution of noisy measures in the accuracy of predictions does increase with s because of the growing of the sum a_s.

It can be shown that $\bar{\boldsymbol{\varepsilon}}_{\eta_{n+1}}$ can increase without bound for the pitch angle θ due to the factors $\left\|\frac{\partial J_j^T(\max|\theta|)}{\partial \boldsymbol{\eta}}\right\|_i$ and $\left\|J(\max|\theta|)\right\|_i$ in (25). The influence of θ could be minimized if $|\theta|$ goes practically below 40 degrees.

6 A complex case study: a ROV

As summarized in the final paragraph of Section 4.3, AB models emerge over the other approximations as quite adequate for control purposes. Once relations between model errors and disturbances in the representation were theoretically established for that approach, we will address ourselves to the evaluation of their features by means of numerical simulation.

We will aim to achieve these goal for a case study employing a ROV with a prescribed control law for the actuators (see Fig. 6). The phenomenological model was taken from a real vehicle (see [8]).

6.1 Set-up

The continuous-time dynamics described in (5), (6) and (7) will be numerically simulated in a forced motion which results from the manipulation of the

8 thrusters (see Fig. 6, to the left) according to prescribed laws. The thruster dynamics is considered parasitic in front of the dominant dynamics of the vehicle.

So, the induced vehicle motion takes place in the form of uncontrolled navigation with and slight ascent due to a positive buoyancy of 1% of its weight

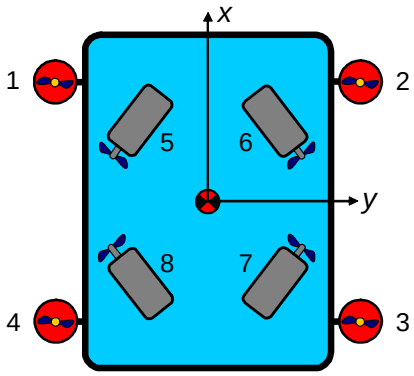

Thruster Number	Mean rpm n_0 (% max rpm)	Sinus variable rpm n_1 (% max rpm) and ω (Hz)
1	-5% (up)	30% / 0.30 Hz
2	-5% (up)	30% / 0.20 Hz
3	10% (down)	15% / 0.15 Hz
4	10% (down)	15% / 0.25 Hz
5	45% (forward)	25% / 0.30 Hz
6	50% (forward)	25% / 0.25 Hz
7	-50% (forward)	25% / 0.15 Hz
8	-45% (forward)	25% / 0.20 Hz

Fig. 6- Set-up for a forced vehicle motion in the case study. Mean and variable rpm values of the thrusters

With the end of accomplishing persistency of excitation to the nonlinear dynamics in every one of its motion modes, we generate the rpm signals of $\mathbf{n}$ as determined by the sum of a mean component n_0 and a sinus component of amplitude n_1 and frequency ω (see Fig. 6, to the right). The simulation time considered was $T = 5000s$ and the error was evaluated from $T = 1000s$ to avoid the transitory error at the beginning of the discrete approximations.

6.2 Results

The results of this case study are summarized in the table below in Figs. 7 for two sampling periods: $h = 0.1$ (s) and $h = 0.5$ (s). It illustrates comparatively the model performance evaluated through the quadratic norm of the disturbed local prediction errors $\bar{\varepsilon}_\eta$ and $\bar{\varepsilon}_v$. These are possible to be computed exactly as indicated in the definition at the start of Section 5.1, due to the availability of the unperturbed measures $\boldsymbol{\eta}(t_n)$ and $\mathbf{v}(t_n)$, and the perturbations $\delta\boldsymbol{\eta}_n$ and $\delta\mathbf{v}_n$ in the simulation. Obviously, this is not possible in a practical case to do when only perturbed measures are available.

The disturbance levels of the noise in the samples are indicated separately as a pair of percentages $(\delta\boldsymbol{\eta}_n\%, \delta\mathbf{v}_n\%)$ in the first column. These quantities indicate a disturbance referred to the magnitudes of 1(m)-30(°) and 1(m/s)-30(°/seg), respectively. The noise samples are generated randomly and added to the sampled states as illustrated in Fig. 1. The characteristic of the noise is like a discrete-time white noise signal with uniform distribution.

In the case study we have employed AB approximations with a small order ($s = 1$, Euler approximation AB1) and a large order ($s = 4$, AB4). The disturbed local errors for position and velocity in the different orders are indicated in the table. They look as an ordered pair of the norms like $(\bar{\varepsilon}_\eta\text{AB1}, \bar{\varepsilon}_\eta\text{AB4})$ and $(\bar{\varepsilon}_v\text{AB1}, \bar{\varepsilon}_v\text{AB4})$, for AB1 and AB4 respectively.

	Sampling period h=0.1 (s)		Sampling period h=0.5 (s)	
Level of noise (δ_η%,δ_v%)	Position error AB1 vs. AB4 ($\bar{\varepsilon}_\eta$ AB1, $\bar{\varepsilon}_\eta$ AB4)	Velocity error AB1 vs. AB4 ($\bar{\varepsilon}_v$ AB1, $\bar{\varepsilon}_v$ AB4)	Position error AB1 vs. AB4 ($\bar{\varepsilon}_\eta$ AB1, $\bar{\varepsilon}_\eta$ AB4)	Velocity error AB1 vs. AB4 ($\bar{\varepsilon}_v$ AB1, $\bar{\varepsilon}_v$ AB4)
(0%, 0%)	AB1 ~ 75xAB4 (1.6×10^{-5}, 2.1×10^{-7})	AB1 ~ 3xAB4 (3.2×10^{-5}, 1.1×10^{-5})	AB1 ~ 1.9xAB4 (7.9×10^{-4}, 4.2×10^{-4})	AB1 ~ 1.8xAB4 (2.2×10^{-3}, 1.2×10^{-3})
(2%, 0%)	AB1 ~ AB4 (1.3×10^{-4}, 1.3×10^{-4})	1.3xAB1 ~ AB4 (3.4×10^{-5}, 4.4×10^{-5})	AB1 ~ 1.6xAB4 (8.3×10^{-4}, 5.0×10^{-4})	AB1 ~ 1.7xAB4 (2.2×10^{-3}, 1.3×10^{-3})
(10%, 0%)	AB1 ~ AB4 (6.4×10^{-4}, 6.4×10^{-4})	3.2xAB1 ~ AB4 (6.6×10^{-5}, 2.1×10^{-5})	AB1 ~ AB4 (1.5×10^{-3}, 1.4×10^{-3})	1.1xAB1 ~ AB4 (2.2×10^{-3}, 2.5×10^{-3})
(20%, 0%)	AB1 ~ AB4 (1.3×10^{-3}, 1.3×10^{-3})	3.6xAB1 ~ AB4 (1.2×10^{-4}, 4.3×10^{-4})	AB1 ~ AB4 (2.7×10^{-3}, 2.8×10^{-3})	1.8xAB1 ~ AB4 (2.4×10^{-3}, 4.4×10^{-3})
(0%, 2%)	1.4xAB1 ~ AB4 (1.8×10^{-5}, 2.6×10^{-5})	1.3xAB1 ~ AB4 (7.9×10^{-5}, 1.1×10^{-4})	AB1 ~ 1.6xAB4 (7.9×10^{-4}, 4.9×10^{-5})	AB1 ~ 1.5xAB4 (2.2×10^{-3}, 1.5×10^{-3})
(0%, 10%)	3.4x AB1 ~ AB4 (3.9×10^{-5}, 1.3×10^{-4})	1.4xAB1 ~ AB4 (3.6×10^{-4}, 5.3×10^{-4})	1.6xAB1 ~ AB4 (8.6×10^{-4}, 1.4×10^{-3})	1.7xAB1 ~ AB4 (2.5×10^{-3}, 4.3×10^{-3})
(0%, 20%)	3.6xAB1 ~ AB4 (7.3×10^{-5}, 2.6×10^{-4})	1.5xAB1 ~ AB4 (7.3×10^{-4}, 1.1×10^{-3})	2.5xAB1 ~ AB4 (1.1×10^{-3}, 2.7×10^{-3})	2.5xAB1 ~ AB4 (3.4×10^{-3}, 8.6×10^{-3})
(2%, 2%)	AB1 ~ AB4 (1.3×10^{-4}, 1.4×10^{-4})	1.3xAB1 ~ AB4 (8.0×10^{-5}, 1.0×10^{-4})	AB1 ~ 1.4xAB4 (8.5×10^{-4}, 6.1×10^{-4})	AB1 ~ 1.4xAB4 (2.2×10^{-3}, 1.5×10^{-3})
(10%, 10%)	AB1 ~ AB4 (6.6×10^{-4}, 7.0×10^{-4})	1.4xAB1 ~ AB4 (3.7×10^{-4}, 5.2×10^{-4})	1.3xAB1 ~ AB4 (1.7×10^{-3}, 2.3×10^{-3})	1.8xAB1 ~ AB4 (2.6×10^{-3}, 4.8×10^{-3})
(20%, 20%)	AB1 ~ AB4 (1.3×10^{-3}, 1.4×10^{-3})	1.4xAB1 ~ AB4 (7.4×10^{-4}, 1.1×10^{-3})	1.4xAB1 ~ AB4 (3.1×10^{-3}, 4.5×10^{-3})	2.6xAB1 ~ AB4 (3.7×10^{-3}, 9.5×10^{-3})
(2%, 20%)	1.9xAB1 ~ AB4 (1.8×10^{-4}, 3.3×10^{-4})	1.5xAB1 ~ AB4 (7.3×10^{-4}, 1.1×10^{-3})	2.4xAB1 ~ AB4 (1.2×10^{-3}, 2.8×10^{-3})	2.5xAB1 ~ AB4 (3.4×10^{-3}, 8.6×10^{-3})
(20%, 2%)	AB1 ~ AB4 (1.3×10^{-3}, 1.3×10^{-3})	3xAB1 ~ AB4 (1.4×10^{-4}, 4.2×10^{-4})	1.1xAB1 ~ AB4 (2.7×10^{-3}, 2.9×10^{-3})	1.8xAB1 ~ AB4 (2.5×10^{-3}, 4.5×10^{-3})

Fig. 7 - Local errors for different orders s of the Adams-Bashforth model and sampling time h

From Fig. 7, when comparing the model performance with respect to s under different degres of disturbances, it is noticing that no apparent advantage is obtained for large-order models over the Euler method. So, the more simple structure is the reasonable choice for controller design in this case.

7 Conclusions

In this paper the adequacy of high order interpolation-based approximations to describe highly perturbed complex dynamics in discrete time was analyzed.

In a first case study, a simple AUV-like ODE system has been utilized. The analysis had established features of the approximations related to modularity, consistency with the model order and degree, accuracy in disturbed contexts with noisy measurements. These features were finally listed for comparison of the

approximations. AB Methods had also shown consistency with increasing order s and do not need intersampling as in the case of the RK approaches. Moreover, the computational efforts of the AB approximations are low, only s times higher that the simplest Euler method. Additionally, the aptitude of the approaches predictions in dynamic behavior was also deemed for digital controller design as ultimate goal. In this sense AB methods had emerged as the most appropriate.

The next step had consisted in the analysis of the sensitivity of local prediction errors to disturbances in the measures under a high signal-to-noise ratio. Here, analytical expressions were determined as a function of physical coefficients of the vehicle like inertia, drag, buoyancy and maneuver parameters.

The disturbances measures were also analyzed. It was found that the contribution of noisy measures in the accuracy of predictions does increase linearly with s and the sampling time period h.

Finally, the results were illustrated with numerical simulations using a ROV model of 6 DoF with complex navigation paths. Special attention was paid on the influence of model parameters like order s, sampling time h and different levels of disturbances both in the position and velocity.

The accuracy of predictions increases exponentially with the order s considering that no disturbance acts on the measurements (both kinematics and spatial). Nevertheless, in presence of noise, no substantial advantage of employing large-order Adams-Bashforth in comparison to the simple Euler approach has been noticed, even when disturbances on the measures are small.

For that reason, even though the arrival of new technology offering extremely good measures not only in velocity but also in position, it is not observed that complex AB model structures may contribute to increase the accuracy of models for controller design. So, the more simple structure of the Euler still is the more reasonable choice for controller design in this complex dynamic.

References

1. T. I. Fossen, *Guidance & control of ocean vehicles*. New York: John Wiley&Sons, 1994.
2. A. V. Inzartev (Editor), *Underwater vehicles*. Vienna, Austria: In-Tech, 2009.
3. P. M., Lee, S. W., Hong, Y. K. Lim, C. M. Lee, B. H. Jeon, J. W. Park, "Discrete-time quasi-sliding mode control of an autonomous underwater vehicle," *IEEE Journal of Oceanic Engineering*, vol. 24, no. 3, pp. 388-395, Jul. 1999.
4. S. Sagara, "Resolved acceleration control for underwater vehicle-manipulator systems: Continuous and discrete time approach," in *Underwater Vehicles*, A.V. Inzartev (Editor). Vienna, Austria: In-Tech, 2009, ch. 23, pp. 437-458.
5. J.R. Dormand, *Numerical methods for differential equations: A computational approach*, Boca Ratón: CRC Press, 1996.
6. E. Hairer, S. P. Nørsett, G. Wanner, *Solving ordinary differential equations I: Non-stiff problems*, Berlin: Springer Verlag,1993.
7. M. A. Jordán and J. L. Bustamante, "A general approach to sampled-data modeling and digital control of vehicle dynamics," in *2009 IEEE Multi-conference on Systems and Control (MSC 2009)*. San Petersburg, Russia, Jul. 8-10, 2009, pp- 159-164.
8. F. Pinto, "Theoretische und experimentelle Untersuchung zur Sensorik und Regelung von Unterwasserfahrzeugen," Ph.D dissertation, Fortschritt-Berichte VDI, Reihe 12, Nr. 292, VDI-Verlag, Düsseldorf.